Effect of ECRH on toroidal rotation in ASDEX Upgrade H-mode discharges

R. M. McDermott, C. Angioni, R. Dux, A. Gude, T. Pütterich, F. Ryter, G. Tardini and the ASDEX Upgrade Team

Max Planck Institut für Plasmaphysik, EURATOM Association, D-85748 Garching, Germany

E-mail: Rachael.M.McDermott@ipp.mpg.de

Abstract. Core toroidal rotation behavior and momentum transport have been examined in neutral beam injection (NBI) heated plasmas with and without electron cyclotron resonance heating (ECRH) in ASDEX Upgrade (AUG). The impurity ion temperature and rotation are measured by means of charge exchange recombination spectroscopy (CXRS) and the main ion rotation is calculated neo-classically based on the measured impurity ion temperature and rotation profiles. In purely NBI heated discharges the plasma spins up in the co-current direction and forms peaked rotation profiles. However, when ECRH power is added to these discharges the rotation decreases significantly leading to flat and occasionally slightly hollow profiles. The rotation at the edge of the plasma ($\rho > 0.65$) is largely unaffected by the application of the ECRH. During ECRH phases the electron temperature in the core increases dramatically concomitant with a flattening of the ion temperature profile. In these phases peaking of the impurity ion and electron density profiles is also observed. The change in toroidal rotation is sensitive to both the amount of ECRH power deposited as well as to the deposition location. The measured rotation changes can not be explained by a modification to the NBI torque deposition profile, a preferential loss of fast ions from the plasma core, or by a simple increase in momentum diffusivity. Additionally, the inward directed Coriolis momentum pinch is predicted to increase, not decrease, during the ECRH phases. Altogether, the data suggest the presence of either an outward convection of momentum or an intrinsic, counter-current directed torque. Although the physics behind these possibilities remains unclear, they are presumably related to either a convective or residual stress driven momentum flux, which responds to the ECRH-induced changes in the plasma profiles and turbulence.

I. Introduction

The realization of the connections between rotation and plasma stability and confinement has made the predictive capability and active control of the rotation profile a critical area of tokamak research. While low confinement mode (L-mode) intrinsic rotation, with its complex behavior, defies simple characterization [1, 2], high confinement mode (H-mode) intrinsic rotation is generally observed to scale with plasma confinement [3, 4]. On some devices access to certain high confinement regimes is linked

to the details of the rotation profile such as in the quiescent H-mode on DIII-D [5] and it is commonly accepted that velocity shear can lead to improved confinement through the suppression of plasma turbulence [6, 7, 8, 9, 10]. This theory is a leading candidate to help explain both the sudden transition from L-mode to H-mode that is observed in most diverted tokamak experiments and the formation of internal transport barriers, which also yield improved confinement. Plasma rotation also plays an important role in the stability of several MHD modes such as resistive wall modes [11, 12, 13, 14], neoclassical tearing modes [15, 16], and edge localized modes [5, 17].

The rotation profile on most contemporary tokamak experiments is dominated by externally applied torque from neutral beam sources, which are used primarily to heat the plasma. The input torque from NBI sources is quite well understood [18]. However, the momentum transport controlling the final rotation profile is not. Although, some recent work has focused on and made some progress toward characterizing this transport [19, 20, 21, 22]. In addition to externally applied torques there are also intrinsic ones, which must also be understood for a complete picture of tokamak rotation. This is especially important for extrapolations to next generation devices, in which the effectiveness of NBI is expected to be diminished. As such, these devices will depend more heavily on alternate heating schemes such as ion and electron wave heating and current drive, both of which have been observed experimentally to impact the plasma rotation [23, 24, 25, 26, 27, 28, 29]. In particular, the influence of electron heating on plasma rotation remains unclear.

Core toroidal rotation changes with the application of ECRH power have been observed previously in DIII-D, JT-60U, and AUG. In DIII-D and AUG it was observed that the application of ECRH power to NBI heated H-modes in certain regimes resulted in a decrease in both the ion temperature and impurity ion rotation profile [30, 24]. These changes were attributed to an enhancement in the ion heat and momentum transport. While this is certainly true, at least in part, it was later observed in DIII-D that the rotation profiles in ECRH heated H-mode plasmas are hollow and in the counter-current direction in the plasma core [23]. This indicates quite clearly the presence of an intrinsic, ECRH triggered, counter-current directed torque; though no satisfactory explanation for this effect has yet been advanced. Similarly, in JT-60U ECRH power was initially observed to cause a flattening of the toroidal rotation profile indicating a change in the plasma transport [31]. However, later it was reported that ECRH increases the momentum diffusivity and convective velocity and also drives intrinsic rotation [26]. The results from these experiments were quite complicated with the intrinsic rotation inside the ECRH deposition radius being directed co-current and the rotation outside counter. The AUG results presented here, though largely in line with previous observations, contribute to the store of information and highlight several new aspects of this phenomenon.

This paper is organized as follows: First, an introduction to the diagnostics and discharges used for this analysis is given in Section II. This includes hardware and data analysis information, as well as details on the heating schemes and relevant plasma

parameters. Section III describes in detail the plasma's response to the application of ECRH power and Section IV presents the observed sensitivities to the level and deposition location of the ECRH power. Section V discusses the available theory and known physical mechanisms that could potentially help to explain the experimental results. In section VI calculations of the intrinsic torque and/or momentum pinch required to fit the data are presented and the key findings and conclusions are summarized in section VII.

II. Experimental Setup

All of the experiments described in this work were carried out on the ASDEX Upgrade tokamak [32]. The impurity ion rotation, temperature, and brightness profiles were measured via the core CXRS diagnostic, which was tuned to image the fully stripped boron population using the B^{4+} spectral line at $\lambda = 494.467nm$. All ion profiles presented in this paper refer to the boron population unless otherwise specified. Dedicated wavelength calibrations using a neon lamp were taken immediately after each experiment to ensure accurate rotation profiles to within a few km/s. The CXRS diagnostic, at the time of the analysis, had fifteen toroidal lines of sight (LOS), which provided complete plasma profiles from the plasma edge to the magnetic axis. All of the CXRS data represent line integrations through one of AUG's neutral heating beams; no inversion was performed on the data. Due to the geometry of the system each LOS had a radial resolution of order $\pm$ 2.5cm. The integration time was limited by the level of CXRS signal and was set to 20ms for all of the discharges included in this analysis. The impurity ion density profiles were determined from the measured CXRS brightnesses and neutral beam density profiles calculated using ADAS cross-sections [33] for both beam stopping and the charge exchange processes.

The electron temperature and density profiles used are from the electron cyclotron emission (ECE) [34] and integrated data analysis (IDA) [35] diagnostics, respectively. The coverage of the ECE system depends on the choice of magnetic field, but typically, with one notable exception discussed in Section IV, covered the full plasma radius for the discharges considered in this work. The IDA diagnostic provides complete electron density profiles by combining measurements from several sources including the edge lithium beam and a five channel interferometer. These density measurements, together with their respective uncertainties, are incorporated into a forward model that determines the most probable, complete, electron density profile.

All of the experiments were performed in nearly identical plasma discharges. An overview of the global plasma parameters for these discharges is shown in Fig. 1. The plasma current, I_p, in each was 600kA and the magnetic field, B_t, was between -2.4 and -2.6T. The negative sign indicates that the magnetic field was in the clockwise direction as seen from a top-down view of the tokamak. Due to the choice of the field and current the edge q was quite high, $q_{95} \simeq 6.5$. The current was chosen to minimize the effect of sawteeth on the rotation and the transport analysis and because the effect of ECRH on

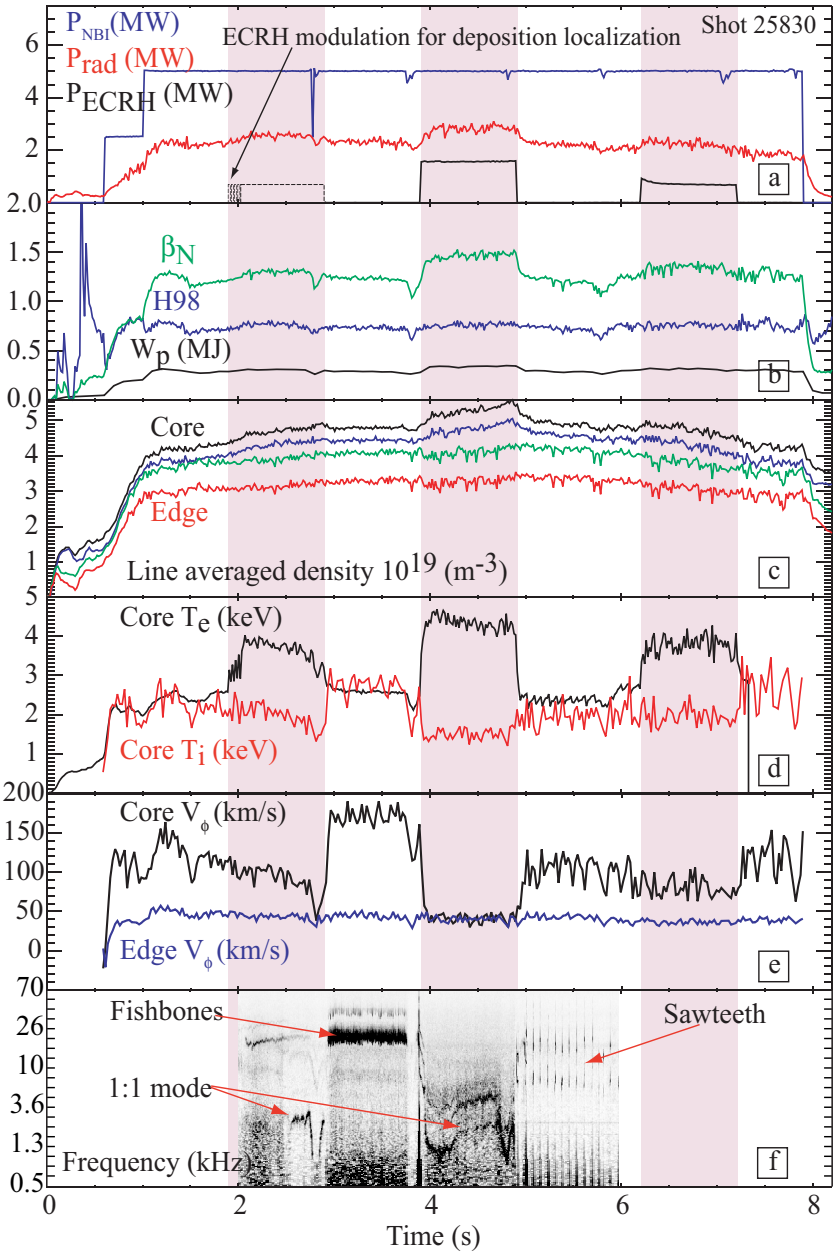

Figure 1. Time traces of global plasma parameters for ASDEX Upgrade H-mode discharge 25830. (a) NBI, ECRH, and radiated power (b) β_N, confinement factor H98, and plasma stored energy W_p (c) Line averaged density from interferometry (d) Core electron and ion temperatures from the ECE and CXRS diagnostics, respectively (e) Core and edge toroidal impurity ion rotation velocities from CXRS (f) Core mode behavior from soft X-ray diagnostic

core rotation is seen most clearly in low current discharges. However, similar results to the ones presented in this work, in terms of the toroidal rotation and ion temperature profiles, have also been observed in 0.8 and 1MA discharges [24]. The discharges were all lower single null (LSN) with an elongation, κ, of 1.66 and fairly low average triangularity, $\delta = 0.24$, where $\delta = (\delta_L + \delta_U)/2$ with $\delta_L \simeq 0.43$ and $\delta_U \simeq 0.04$.

An example of the type of heating scheme used for these discharges can be seen in Fig. 1(a). A combination of NBI and ECRH heating was used for all of the discharges considered. Each discharge was heated continuously with either 2.5 or 5MW of NBI power. In all cases the beam source viewed by the CXRS diagnostic was on for the entire discharge to allow for continuous measurements. The NBI system on AUG is comprised of eight 2.5MW beam sources with different toroidal injection angles. By employing different combinations of these sources it is possible to vary the applied NBI torque density profile and hence, the initial rotation profile. This technique was employed in these experiments to maximize the number of different beam power, ECRH power, and torque density profile combinations. For each beam configuration a 0.5 to 1s long ECRH pulse of 0.6 to 2.2MW was added once the plasma had come to an equilibrium as indicated by the red highlighting in Fig. 1. The ECRH system was configured for X-mode second harmonic heating at 140GHz [36] and the deposition location was set using steerable mirrors. The actual deposition location was confirmed by briefly modulating the ECRH power and looking at the amplitude and phase of the resultant modulation in the ECE measured temperature profiles. An example of this modulation can be seen in the first ECRH pulse shown in Fig. 1(a). All of the data presented in this work came from discharges with nearly on-axis ECRH heating with the exception of the deposition location scan presented in Section IV. In all cases the geometries of the ECRH gyrotrons used were balanced such that the amount of current driven was negligible.

In these discharges the L-H power threshold was roughly 1.5MW making the 2.5MW from a single beam source more than sufficient to initiate H-mode. The confinement scaling factor, H98, for these discharges is shown in Fig. 1(b) and was typically around 0.8; demonstrating the relatively poor H-mode confinement achieved. The principal effects of adding ECRH power to these plasmas, which will be discussed in detail in section III, can be seen in the time traces presented in Figs.1(c-e). In panel (c) one can see a peaking of the core electron density on the innermost interferometry channels when sufficient ECRH power is added. Panels (d) and (e) illustrate the dramatic changes in the core temperature and rotation profiles that occur when ECRH power is applied; namely, a significant increase in the core electron temperature together with sharp decreases in the core ion temperature and rotation. Note, that the edge rotation, shown in blue in panel (e), remains unaffected.

During the NBI only phases of these discharges either fishbone or sawtooth instabilities were routinely observed, see Fig. 1f. However, during the ECRH phases these instabilities disappeared, possibly due to a local change in the q profile from changes in the core temperature profiles, and were replaced by a low frequency ($\simeq$2kHz) mode seen on the soft x-ray diagnostics and diode bolometry data. The mode appears

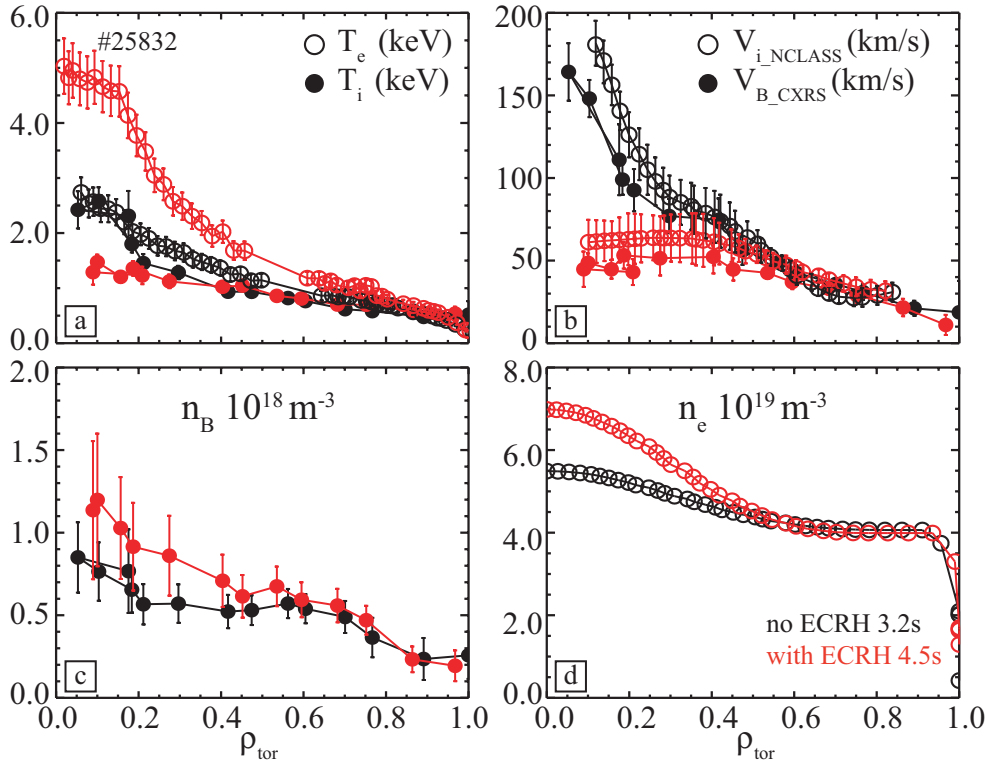

Figure 2. Comparison of ion and electron temperature (a), deuterium and boron toroidal rotation (b) and boron and electron density (c and d) profiles in a 5MW NBI heated discharge with and without 2MW of central ECRH power. The electron temperature and density profiles are from the ECE and IDA diagnostics, respectively. The boron profiles are from the core CXRS and the deuterium rotation was calculated from NCLASS using the measured boron rotation and temperature profiles as inputs.

to be a weak n:m =1:1 kink (n and m are the toroidal and poloidal mode numbers) and is well localized inside of $\rho_{tor} = 0.21$, where ρ_{tor} is the normalized toroidal flux radius. Due to the strength and the core localization of the mode it is unlikely that it can effect significant radial transport, and thus, impact the transport analyses presented in this work.

III. Plasma Response to ECRH Power

In purely NBI heated discharges the core ion and electron temperatures tend to be quite similar. However, as can be seen in Figs. 1d and 2a, the addition of electron heating breaks the agreement. The core electron temperature and temperature gradient increase significantly concomitant with a drastic decrease and flattening of the ion temperature profile. The change in the electron profile is the result of the direct heating, while the change in the ion profile is due mainly to a large increase in the ion thermal diffusivity. This must be the case since the total heating power to the ions is largely unchanged between the non-ECRH and ECRH phases. The extreme changes in these profiles lead to values of T_e/T_i greater than 2 in the core of these H-mode discharges.

The electron and impurity ion density profiles, see Figs. 1c and 2c-d, also react to the addition of the ECRH. The electron density profile, initially only moderately peaked, is observed to peak further with the largest change in the density gradient being around mid-radius. In the purely NBI heated phases the normalized electron density gradient, $\mathrm{R/L}_{n_e} = R|\nabla n_e/n_e|$, is approximately equal to 2 at mid-radius. With the highest levels of ECRH power ($\mathrm{P}_{ECRH} \sim 2MW$) $\mathrm{R/L}_{n_e}$ can be as high as 4 at the same location. Here, R is the flux surface averaged major radius, which is approximately equal to 1.7m for ASDEX Upgrade. The impurity ion density profiles behave similarly to the electrons. In the phases with NBI heating only the impurity profiles at mid-radius are flat or even slightly hollow. However, with ECRH they are also observed to peak increasing by of order 50% in the plasma core.

The peaking of the density profiles in these plasmas is in contrast with the flattening that is often observed in plasmas with central electron heating [37, 38, 39, 40]. However, a detailed analysis of the electron and boron particle transport at mid-radius in these plasmas show that the experimental behaviors are well described by the theoretical modeling [41]. The behavior of the electron density is consistent with the theoretical predictions for ITG turbulence [42] and the boron density behavior also appears to be consistent with theory if the term in the impurity flux expression proportional to the gradient of the plasma rotation is included in the calculations [43].

The most dramatic changes can be seen in the toroidal rotation profiles. In purely NBI heated discharges the plasma spins up in the direction of the beams (standard beam direction is co-current) and forms peaked rotation profiles. The exact shape and magnitude of the profiles varies with the choice of beam configuration. When ECRH power is added to the discharges considered here the rotation decreases significantly leading to flat and occasionally even slightly hollow profiles. To date, the core rotation has not been observed to actually go counter-current. An example of the change in the toroidal rotation with ECRH power is shown in Fig. 2b and the time trace presented in Fig. 1e demonstrates the perfect correlation between the change in rotation and the application of the ECRH. This large change in the core plasma rotation has also been corroborated by a similar change observed in the frequency of the core mode described in Section II and shown in Fig. 1f.

The change in the core rotation can be as large as 100km/s and the effect normally extends over more than half of the plasma radius ($0 < \rho_{tor} < 0.6$). In the highest ECRH power cases ($\mathrm{P}_{ECRH} \sim 2\mathrm{MW}$) the change in rotation is observed to extend all the way to the top of the pedestal. However, for $\mathrm{P}_{ECRH} < 1.5\mathrm{MW}$ the edge profiles appear entirely unaffected as can be seen by examining the edge toroidal rotation trace in Fig. 1e. Here, one can also see how truly flat the profiles become by noting that the core and edge rotation are identical in the high ECRH power phase (4-4.9s). Based on these observations, the change in the toroidal rotation appears to be entirely a core effect most likely linked to either the ECRH induced changes in the plasma turbulence or temperature profiles. With the available temporal resolution (20ms) no propagation from or toward the plasma edge is observed.

The main ion toroidal rotation profiles were calculated with the neoclassical code NCLASS [44] using the measured impurity ion temperature and toroidal rotation profiles as inputs. The main ion rotation shows very similar behavior to the impurity ion rotation, beginning with peaked profiles in the NBI phases and collapsing with the application of the ECRH. The profiles are particularly similar for the high power ECRH cases, in which the gradients of the ion temperature profiles are small. In these discharges, the gradients of the main ion and impurity ion rotation profiles were nearly identical. A comparison of the measured boron and calculated deuterium rotation profiles is shown in Fig. 2(b). Here, one can see the similarities in shape, magnitude, and behavior between the two sets of profiles.

The time scales on which different parameters respond to the application or removal of the ECRH power help to identify the important quantities governing the plasma behavior. The electron temperature profile responds almost instantaneously ($< 1ms$) to the application (or removal) of ECRH power, but takes of order 40-60ms to reach its new steady state profile. The change in the electron density profile, however, is delayed from the onset of the ECRH power by of order 10ms. Once it begins to change it too takes of order 40-60ms to reach a steady state profile. This delay supports the idea that the change in the electron temperature profile is a direct result of the applied heating while the change in the electron density is a transport effect caused by the change in other plasma parameters. Unfortunately, the time resolution of the CXRS diagnostic prevents this sort of analysis for the impurity ion profiles. However, these profiles also reach their final state on the same time scale, i.e. within 60ms after the ECRH is turned on or off. Future experiments with higher CXRS temporal resolution may shed more light on the relative time scales between the change in rotation and the changes in the ion and electron temperature profiles.

IV. Sensitivity to Power Level and Deposition Location

The change in toroidal rotation is sensitive to both the amount of ECRH power deposited as well as to the deposition location. The latter was tested using a series of three identical discharges in which the ECRH deposition location, ρ_{ECRH}, was scanned shot-to-shot from ρ_{tor}=0.4 to ρ_{tor}=0. The level of power (1.1MW) was kept constant for all three discharges. The results from this experiment can be seen in Fig. 3. The rotation profiles before the application of the ECRH, Fig.3a, overlay very well indicating that the initial conditions for all three discharges were indeed very similar. The final rotation profiles after the application of the ECRH are shown in Fig. 3b. With the deposition at mid-radius (blue) no change is observed in the rotation profiles and when the ECRH is moved further inward to ρ_{tor}=0.2 (green) only a slight change is observed ($\sim$20km/s) inside of the deposition radius. However, when the ECRH power is placed on axis (red), the rotation profile collapsed by roughly 80km/s in the core forming a hollow profile.

It seems likely that the rotation behavior is linked to the ion and electron temperature profiles (Fig. 3(c)) most likely through the resultant changes in the plasma

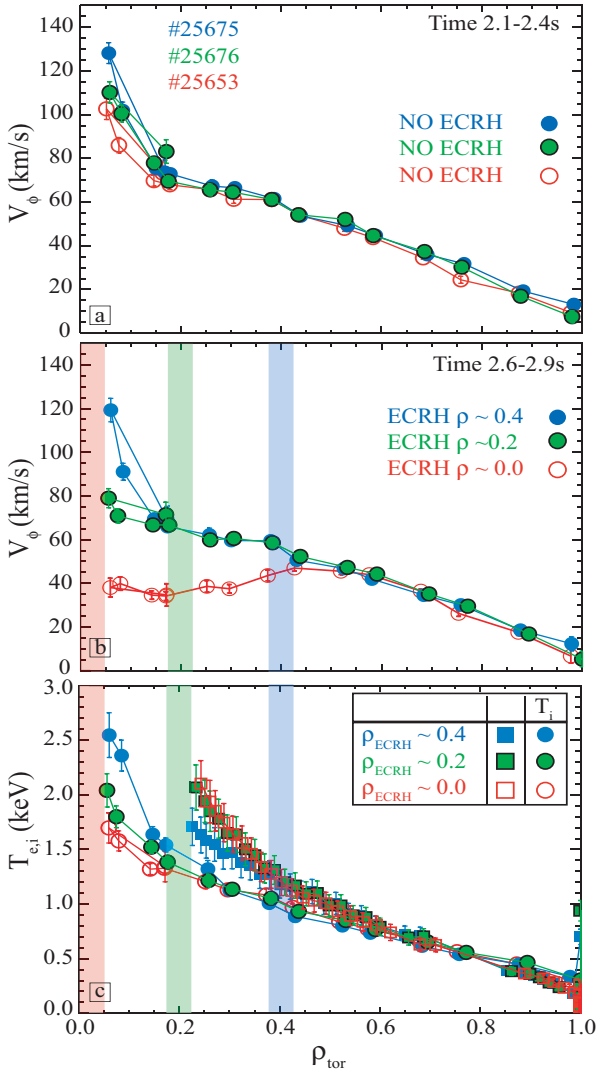

Figure 3. Rotation and temperature profiles from three discharges in which 1.1MW of ECRH power was scanned shot-to-shot from 0.4> ρ_{tor} >0.0. (a) The initial rotation profiles (no ECRH) from the three discharges overlay well indicating similar starting conditions. (b) The final rotation profiles (with ECRH) show a clear dependence on the ECRH power deposition location.(c) The ion temperature profiles (circles) show a small but distinct change with the ECRH deposition radius, while the electron temperature profiles (squares) are inconclusive due to incomplete profiles.

turbulence. The electron temperature and temperature gradient increased during the ECRH pulses for all three discharges, but were clearly higher for the $\rho_{ECRH} = 0$ and 0.2 cases than for $\rho_{ECRH} = 0.4$. However, there was no discernible difference between the T_e profiles in the $\rho_{ECRH} = 0$ and ρ_{ECRH}=0.2 discharges. One should note that in these discharges, due to the slightly higher magnetic field used (-2.6T), the ECE diagnostic did not have full coverage of the plasma core. Rather, the T_e profiles only extend in to $\rho_{tor} = 0.25$. The magnetic field setting was chosen so that the ECRH could be deposited fully on-axis, which is not possible with the lower field. Unfortunately, it was not possible to have very central ECRH deposition and measure complete electron

temperature profiles with the ECE diagnostic at the same time. This capability should be available in future campaigns. It is possible, even likely, that the electron temperature profiles differed inside of $\rho_{tor} = 0.25$ where the actual electron heating was taking place. The ion temperature profiles were available over the complete plasma radius and show a slight, but reproducible, difference between the three cases. For all three deposition locations the ion temperature was observed to flatten similar to the behavior shown in Fig. 2a. However, the change was greatest for the on-axis case and became progressively weaker for the off-axis cases as shown in Fig. 3c. This means that the central value of T_e/T_i also became progressively higher as the deposition location was moved further inward.

These data suggest a correlation between the change in core rotation and the ion or electron temperature profiles, or perhaps the ratio of T_e over T_i. If this is the case then higher levels of off-axis ECRH power should be able to alter the gradients sufficiently to observe a change in the toroidal rotation. This hypothesis is further supported by the sensitivity of the rotation change to the level of ECRH power. This was examined by looking at the rotation profiles from plasmas with identical parameters and beam configurations, but varying levels of centrally applied ECRH power. The flattest and in some cases most hollow rotation profiles are obtained for the highest levels of ECRH power. A similar relationship is observed in the ion temperature profile, while the electron temperature and T_e/T_i increase with the level of ECRH power. These relationships are demonstrated clearly in Fig. 4, which shows the normalized gradient scale lengths of the ion and electron temperature profiles, $R/L_{T_{e,i}} = R|\nabla T_{e,i}/T_{e,i}|$ and the ratio of the electron to ion temperature at $\rho_{tor} \sim 0.3$ as a function of the applied ECRH power. Here, the near perfect opposing symmetry of the ion and electron temperature gradients as a function of the applied ECRH power, which results in a linear relationship between T_e/T_i and P_{ECRH}, is quite striking.

The hypothesis that the rotation change is connected to the ECRH induced changes in the temperature profiles is also consistent with it being a core effect localized to the area in which the changes in the temperature profiles are greatest. The correlation between temperature profiles and rotation can be examined directly by comparing the gradient of the toroidal rotation to the normalized electron and ion temperature gradient scale lengths. Fig. 5 shows this comparison at ρ_{tor}=0.26. Here, the gradient of the rotation has been normalized by the major radius over the local thermal velocity. In Fig. 5(a) one sees a perfect linear correlation between the gradients of the toroidal rotation and the ion temperature, while in Fig. 5(b) there is a clear separation of peaked and flattened rotation profiles with decreasing L_{Te} or increasing T_e/T_i. The flat and hollow rotation profiles seem to occur only for R/L_{Te} above 8, which corresponds to a T_e/T_i ratio of $\sim$1.3. Very similar results are obtained for all minor radii inside of ρ_{tor}=0.45. From these relationships, and a direct examination of the data, it is clear that the flattest and most hollow rotation profiles correlate with the steepest electron temperature gradients and the highest values of T_e/T_i.

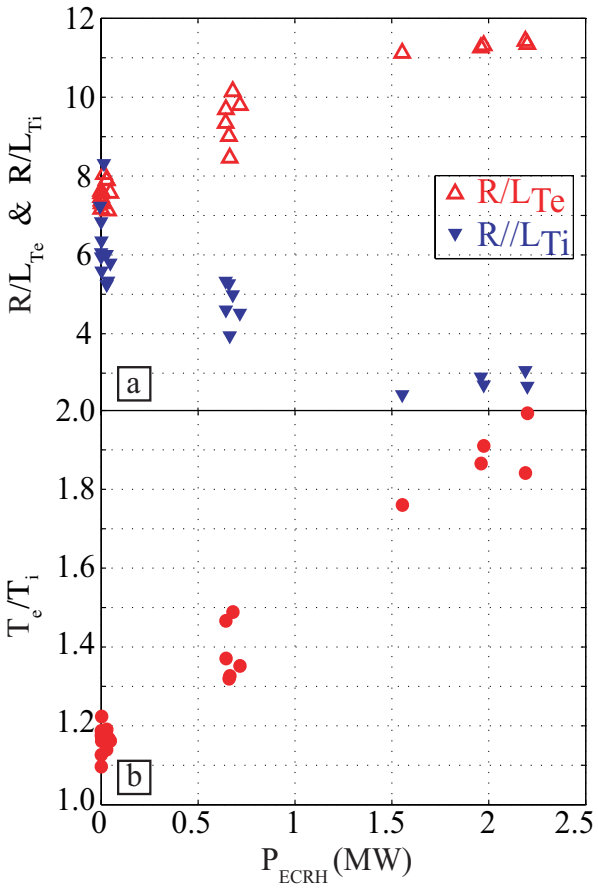

Figure 4. Normalized gradient scale lengths of the ion and electron temperature profiles (a) and the ratio of the electron to ion temperature (b) at ρ_{tor} ~0.3 as a function of centrally applied ECRH power.

V. Discussion

Several possibilities to explain the observed rotation behavior have been considered. First, the flattened ion temperature and rotation profiles can be explained in part by a simple, albeit large, increase in the ion thermal and momentum diffusivities, χ_i and χ_ϕ. This explanation is obviously insufficient to explain hollow rotation profiles, however, many of the rotation profiles are merely flat, not hollow. If the transport is assumed to be purely diffusive then the requisite diffusivities can be calculated according to

$$\Gamma_m = -n_e m_{eff} \chi_{eff} \frac{d\langle V_\phi \rangle}{dr}. \quad (1)$$

Here, Γ_m is the momentum flux, n_e is the electron density, m_{eff} is the effective ion mass given by $\sum_i (m_i n_i / n_e)$, V_ϕ is the toroidal rotation, r is a flux surface averaged minor radius, and χ_{eff} is the effective momentum diffusivity. This effective momentum diffusivity, χ_{eff}, differs from χ_ϕ only in that it assumes there are no additional terms in the momentum equation. For this, and all subsequent calculations, it was assumed that $V_\phi = \omega_\phi R$, where the toroidal rotation frequency, ω_ϕ, is constant on a flux surface [45].

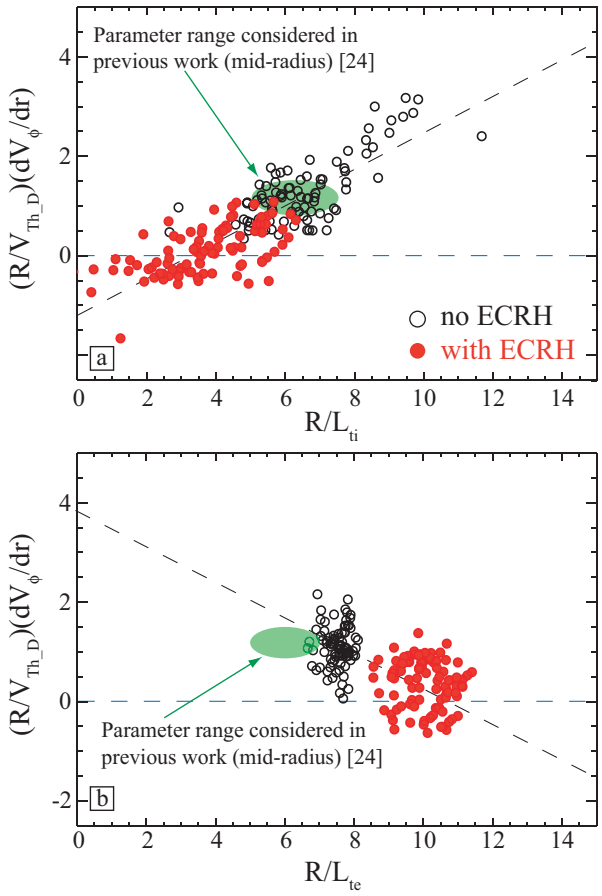

Figure 5. The gradient of the toroidal rotation normalized by the major radius over the ion thermal velocity versus the normalized gradient scale length of the ion (a) and electron (b) temperature profiles at ρ_{tor}=0.3. Black symbols indicate NBI heating only and red symbols are from phases with both NBI and ECRH power. Note, negative values indicate hollow rotation profiles. The green highlighted regions represent the parameter ranges obtained in previous works at mid-radius [24].

The results of this calculation for one of the discharges considered in this analysis are shown in Fig. 6. The calculation was performed using both the measured impurity ion rotation profiles and the TRANSP [33] calculated main ion profiles and yielded nearly identical results for both. The χ_{eff} shown in Fig. 6 is the momentum diffusivity calculated with the deuterium rotation profiles. It should be noted that in many cases the uncertainties in the gradient of the rotation profile are very large and the derived momentum diffusivities had to be considered with care. Despite this difficulty, it was determined that the data sets with low levels of ECRH power or high levels of on-axis beam heating, which have the strongest central torque deposition, can be explained fully by reasonable increases in diffusivity with effective Prandtl numbers (Pr $=\chi_{eff}/\chi_i$) of order 0.5-1. This is consistent with many previous experimental results, which have shown that the ion heat and momentum transport channels are linked [46, 47, 18, 48, 52]. Examples of these two conditions can be seen in the first and third ECRH phases shown in Fig. 6. In the first ECRH phase there are 2.5MW of central beam heating and 0.7MW

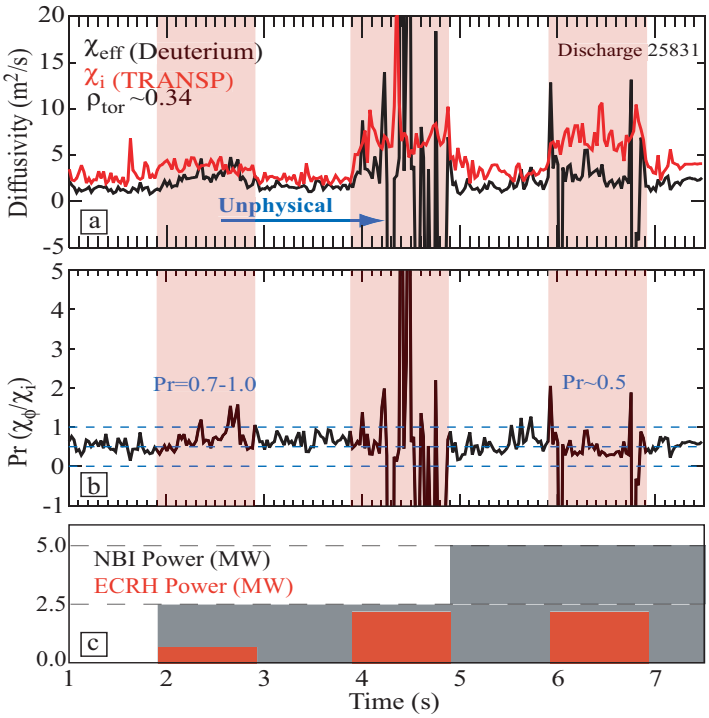

Figure 6. (a) The effective momentum diffusivity (black) and the TRANSP [33] calculated ion thermal diffusivity (red) at ρ_{pol} ~0.34 required to explain the observed rotation and ion temperature profiles assuming purely diffusive transport. (b) Prandtl number resulting from the calculated diffusivities (c) Schematic of the NBI and ECRH heating schemes used in this discharge (25831).

of central ECRH heating. In this case both χ_i and χ_{eff} show very modest increases above the purely NBI heated phases leading to Prandtl numbers approaching 1. In the third ECRH phase the central beam and ECRH power have been increased to 5 and 2.2MW, respectively. Here, the transport in the ion heat channel is increased by the addition of ECRH power as indicated by the increase in χ_i, but the momentum transport is still dominated by the neutral beam input and the χ_{eff} is relatively unaffected. This can be seen in the rotation profiles themselves, which under these conditions, are lower than in the purely NBI phases, but maintain a similar radial gradient.

In contrast, when the ECRH power is high and the central beam torque is low, the observed rotation profiles are very flat or even slightly hollow. In these cases, momentum diffusivities as large as $100\mathrm{m}^2/\mathrm{s}$ (Pr ~10) are needed to explain the rotation profiles, while the hollow rotation profiles, of course, result in non-physical, negative diffusivities. This is the case for the second ECRH phase in Fig. 6. Here, the rotation profiles fluctuate between very flat and hollow leading to calculated effective diffusivities that fluctuate between very high and negative values. Therefore, although an increase in the momentum diffusivity certainly plays a significant role in determining the final rotation profile, it can not be the only mechanism at work.

As a partial explanation it was suggested that the drastic changes in the temperature profiles, and more modest changes in the density profiles, could change

the beam torque deposition profile in the ECRH phases, leading to altered rotation profiles. This possibility was refuted through comparison of the TRANSP calculated torque deposition profiles from ECRH and non-ECRH phases of several discharges with different beam configurations. In all cases the deposition profiles are virtually identical between the different heating phases.

Linear GS2 runs [50, 51] were performed for several of the discharges to examine the dominant instabilities and to compare the magnitudes of the Coriolis momentum pinch [49] in the ECRH and non-ECRH phases. The GS2 runs indicate, as expected, that the dominant mode moves from ion temperature gradient modes (ITG) toward trapped electron modes (TEM) when ECRH power is applied. For the highest ECRH power cases ($\sim$2MW) the mode actually switches to TEM in the plasma core. However, it remains unclear how electron modes could produce the high levels of ion heat and momentum transport that are observed in these discharges. The GS2 calculation of the Coriolis pinch at mid-radius ($\rho_{tor} = 0.5$) are shown in Fig. 7. Here, the results have been broken down into three data sets depending on the heating scheme. Blue squares indicate data taken from purely NBI heated plasmas, green triangles come from phases with NBI and low levels of ECRH power, and red triangles are from phases with NBI and high levels (>2MW) of ECRH power. The inward directed Coriolis pinch velocity, V_{cor}, is shown in Fig. 7(b) and very clearly increases with increasing ECRH power and T_e/T_i leading, theoretically, to more peaked rotation profiles rather than less, which is in direct contradiction with the measurement. The increase in the Coriolis pinch is expected since it depends primarily on the gradient of the electron density, which is observed to peak in the ECRH phases of these discharges. In Fig. 7(b), the pinch has been normalized by the momentum diffusivity, or equivalently the ion diffusivity, since the Prandtl number calculated by GS2 remains roughly equal to 1 for all three heating scenarios, see Fig. 7(a).

It is possible that a change in the beam delivered fast ion distribution could help to account for the change in rotation profiles. If the fast ions are transported out of the core by MHD activity before they can impart their energy and momentum then this could account for both lower ion temperature and rotation profiles. However, almost no mode activity was observed during the ECRH phases of the discharge with the exception of the very low frequency mode mentioned in Section II. This mode was very difficult to observe as it was very localized to the plasma core ($\rho_{tor} < 0.21$) and because the signal was almost lost in the low frequency noise. Due to the localization of this mode it is unlikely it can be responsible for the large scale plasma heat and momentum transport, which extends across more than half of the plasma radius. In addition, there is no evidence for a change in the fast ion distribution with ECRH power. The neutron rate increases by roughly twenty percent during the ECRH phases, but this increase can be correlated with the corresponding increase in the plasma density. Further, a comparison of the measured and TRANSP calculated neutron rates shows remarkably good agreement, well within the error bars of the measurement. Hence, the changes in plasma rotation can not be explained by radial transport of fast ions out of the plasma

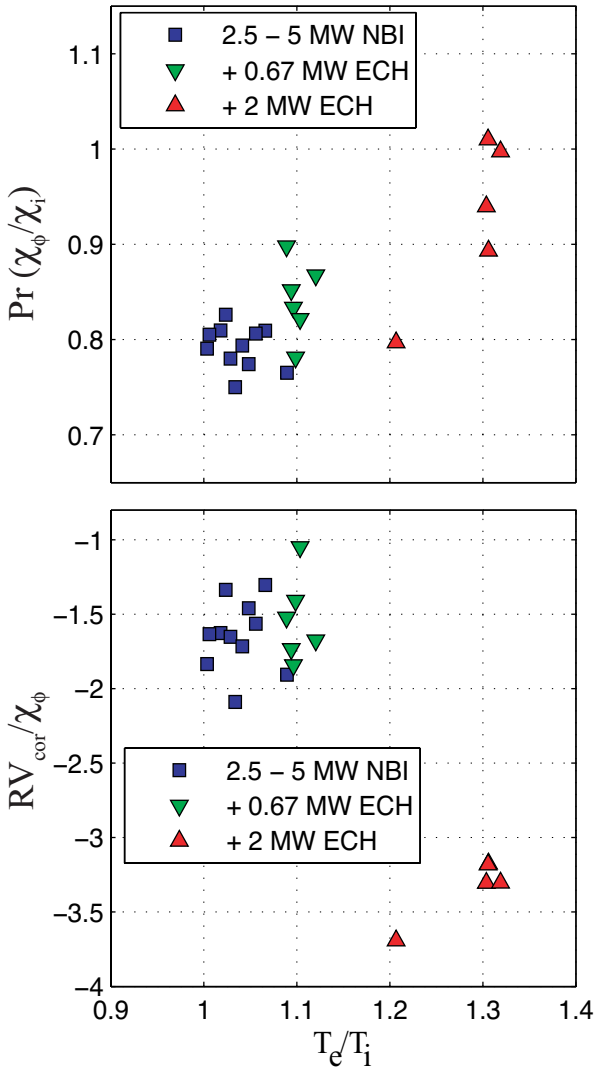

Figure 7. (a) Linear GS2 calculations of the ratio of the Prandtl number and (b) the Coriolis pinch velocity normalized by χ_{phi} as a function of the electron to ion temperature ratio at mid-radius ($\rho_{tor} \sim 0.5$) for three different heating schemes.

core.

Lastly, it is possible for modes to directly brake the plasma rotation through interaction with the vessel walls. However, the core localization of the only modes observed in these plasmas make this possibility unlikely. In addition, the edge magnetic diagnostics did not observe any perturbations connected to these modes, indicating that this was not taking place.

The changes in the core toroidal rotation profiles with ECRH power can not be explained solely by an increase in the momentum diffusivity. Additionally, the other mechanisms considered do not help to explain the observations. In particular, the change in the Coriolis momentum pinch actually acts to increase the core rotation. Altogether, the AUG data suggest the presence of either an ECRH triggered outward momentum pinch or intrinsic, counter-current directed torque. Taken together with the results from

other devices [23, 26], the counter-current directed torque is more likely. The authors do not mean to imply that ECRH power can apply a direct torque on the plasma. The interaction of electron cyclotron waves with plasmas is quite well understood and there is no way for ECRH heating to impart significant momentum directly to the plasma. Rather, the physical mechanism behind the rotation changes, while unknown, is presumed to be related to a convective or residual stress driven momentum flux triggered by the ECRH induced changes in the core temperature profiles and plasma turbulence.

At this point it is worthwhile to compare the findings presented here to similar results observed previously on AUG in the context of electron and ion heat transport studies [24, 53]. In these studies several MW of ECRH power were also added to H-mode plasmas heated with a background of 5MW NBI power. In these discharges the addition of the ECRH increased the core T_e and decreased the core T_i and V_ϕ profiles similarly to what is seen here. However, the changes were not nearly as dramatic and did not lead to flattened ion temperature or rotation profiles. The mid-radius rotation gradient (normalized by the major radius over the thermal velocity) for these discharges remained between 1 and 1.4 (strongly peaked) for all cases even those with the highest levels of ECRH power. The parameter ranges achieved in the older set of discharges are highlighted in green in Fig. 5 and can be compared to the parameter ranges obtained in the present work (black and red). One should note that Fig. 5 does not present an entirely fair comparison as the radial locations at which the gradients of the profiles are analyzed differ between the present and former data-sets. However, as mentioned earlier, in the present data set similar parameter ranges (particularly for the rotation and ion temperature profiles) are obtained for all radii between $\rho_{tor} = 0.2$ and 0.45 and so Fig. 5 serves well to illustrate the drastically different temperature and rotation gradients obtained in the two sets of discharges.

The primary differences between the former discharges and the present are the plasma current and the achieved energy confinement. The present discharges were performed at 600kA and typically had poor H-mode confinement (H98$\sim$0.8). The former were run at 1MA and had significantly higher energy confinement (1<H98<1.3). It is the opinion of the authors that the difference in confinement is the principal factor leading to the altered behavior. In the older discharges the higher energy confinement resulted in higher initial T_i profiles in the NBI only phases giving T_e/T_i values in the range of 0.5 to 0.7. The addition of the ECRH power increased the ion transport and heated the electrons, thus lowering T_i while increasing T_e and pushing the plasma into a T_e/T_i range of ~ 1 [24]. Within the working theory that the observed changes in rotation are the result of a combination of increased ion transport (higher $\chi_{i,\phi}$) from the additional heating power and an additional mechanism connected to the drastic changes in the temperature profiles, particularly to high T_e/T_i, the previous results are not inconsistent with the current observations.

VI. Calculation of Required Torque or Outward Pinch

Although the actual physical mechanism affecting the plasma rotation can not, at this time, be determined, the magnitude of the missing term(s) in the toroidal momentum conservation equation can be estimated. Two possibilities will be considered in this section: first, that the ECRH induced effect can be modeled as an outward pinch term and second, that it can be modeled as intrinsic counter-current directed torque of unknown origin. Assuming the first, the momentum conservation equation can be written as

$$\int (S_{NBI})\, dVol = -m_{eff} n_e R \left\langle \frac{\partial Vol}{\partial r} \right\rangle \left[\chi_\phi \frac{\partial \langle V_\phi \rangle}{\partial r} - V_c \langle V_\phi \rangle \right], \tag{2}$$

where S_{NBI} is the NBI delivered torque density, Vol is the plasma volume, V_C is the desired total convective velocity, which includes both the Coriolis pinch and an anomalous contribution, and the other quantities are defined as in equation 1. The total convective velocity can be calculated by using TRANSP computed torque density profiles and assuming that $\chi_\phi \simeq \chi_i$ [46, 47, 18, 48, 52]. It only makes sense to perform this calculation for cases where the profiles can not be explained by a reasonable increase in χ_ϕ and at radii where a change in the toroidal rotation is actually observed. Hence, the results presented here focus on the central region of the plasma ($\rho_{tor} < 0.5$) and apply only for cases of high ECRH power and relatively low central torque such as in the second ECRH phase of discharge 25831, see Fig. 6. An example of the results from this calculation is shown in Fig. 8. The profiles plotted here are averaged over steady portions of the discharge and the error bars represent only the standard deviation observed in the calculation during this period. In the NBI phases of the discharge V_C is found to be negative (inward) across the entire profile, of order 1-2m/s in the plasma core and larger (5-10m/s) toward the outer-half of the plasma. When ECRH is added to the discharges the pinch velocity in the core becomes slightly positive (outward) while outside mid-radius it remains in the inward direction. This can be compared with the Coriolis pinch as calculated by the linear runs of GS2. The results of these calculations are indicated by the diamonds in Fig. 8. During the non-ECRH phase, the GS2 results indicate an inward pinch of similar magnitude, though a bit smaller, than the convective velocity calculated via equation 2. During the ECRH phase the GS2 predicted Coriolis pinch increases in the inward direction across the entire profile, becoming slightly larger than the calculation at mid-radius and giving a clearly negative contribution to the total convective velocity in the plasma core. This indicates that the anomalous contribution to the total convective velocity would have to be centrally localized and strongly outward.

Alternatively, it can be assumed that the application of the ECRH triggers a non-negligible intrinsic torque (S_{ECRH}), which must be included in the momentum conservation equation. In this case equation 2 can be re-written as

$$\int (S_{NBI} + S_{ECRH})\, dVol = -m_{eff} n_e R \left\langle \frac{\partial Vol}{\partial r} \right\rangle \left[\chi_\phi \frac{\partial \langle V_\phi \rangle}{\partial r} - V_c \langle V_\phi \rangle \right]. \tag{3}$$

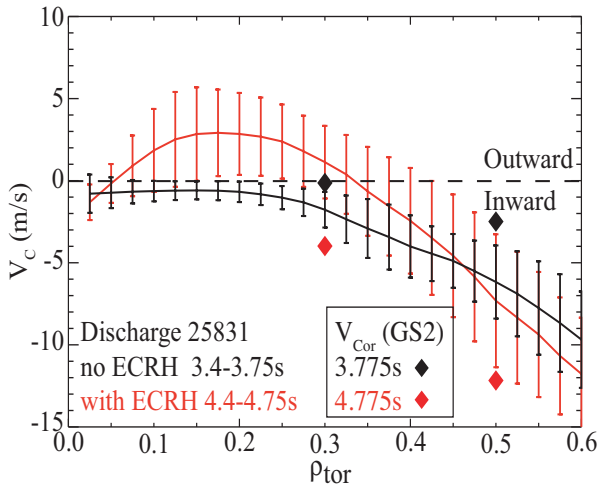

Figure 8. Calculated convective velocity according to Eq. 2 for two phases of discharge 25831, one with ECRH (red) and one without (black). The diamonds indicate calculations of the Coriolis pinch by linear runs of GS2 for the same discharge and in the same time ranges.

To estimate the intrinsic torque equation 3 was solved by again assuming that $\chi_i = \chi_\phi$ and by using two different assumptions for the convective velocity. First, the convective velocity was determined via equation 2 for the non-ECRH phases of the discharge and was assumed to stay constant during the ECRH pulses. Second, it was assumed that the convective velocity increases proportionally to the ion (and momentum) diffusivity. This assumption is qualitatively consistent with the trend predicted by the calculations of the Coriolis pinch. Sample results from the same discharge used for the calculations shown in Figs. 6 and 8 are shown in Fig. 9. The blue curve shows the resultant torque assuming a constant convective velocity and the red curve corresponds to the calculation using the scaled velocity. Both assumptions produce ECRH induced torque profiles that are negative in the core and are effectively zero outside of $\rho_{tor} = 0.4$. The assumption that the pinch term, which is always inward, increases proportionally to χ_i obviously results in higher core ECRH induced torques. In both cases the magnitude of the needed torque density is on the same order of magnitude as that delivered by the neutral beams.

The calculations described in this section were performed with both the measured impurity ion rotation profiles as well as the NCLASS calculated main ion profiles and the results were found to agree reasonably well. The profiles shown in Fig. 8 and Fig. 9 were calculated using the impurity profiles, which were chosen because they provide a smoother data set and yield cleaner results. The ECRH induced torques and convective velocities presented in this section do not necessarily represent the actual behavior occurring in the plasma discharges. Rather they seek only to estimate, based on reasonable assumptions, the magnitude and direction of additional terms in the momentum conservation equation that could describe the experimental observations.

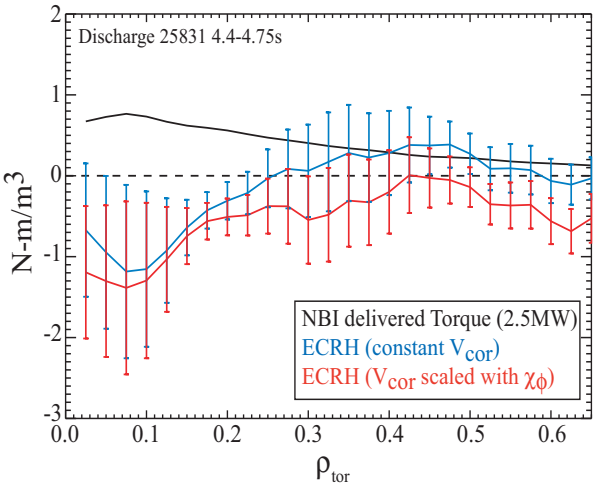

Figure 9. Applied NBI torque density (black) and intrinsic torque densities (blue and red) calculated via Eq. 3 for the second ECRH phase of discharge 25831. The blue curve was calculated assuming that V_C remains unchanged from the NBI only phase of the discharge, and the red curve assuming that it increases proportional to the TRANSP calculated ion thermal diffusivity.

VII. Summary and Conclusions

Dramatic decreases in the core toroidal rotation profiles are observed when ECRH power is added to low current, moderate density NBI heated H-mode discharges in the ASDEX Upgrade tokamak. In purely NBI heated discharges the plasma spins up in the co-current direction and forms peaked rotation profiles. However, when sufficient ECRH power is added to these discharges the rotation decreases significantly leading to flat and occasionally even slightly hollow profiles. During ECRH phases the electron temperature in the core increases dramatically concomitant with a flattening of the ion temperature profile. Additionally, a modest peaking of both the boron and electron density profiles is observed. The change in the core toroidal rotation (also $T_{e,i}$ and $n_{e,B}$) is sensitive to both the amount of ECRH power deposited as well as to the deposition location possibility through the corresponding changes in the ion and electron temperature profiles. The most dramatic changes were observed with the highest power levels and almost no change in rotation was observed with off-axis power deposition.

The measured rotation changes can not be explained by a simple increase in momentum diffusivity, a modification to the NBI torque deposition profile, a preferential loss of fast ions from the plasma core, or an interaction of core modes with the vessel wall. Additionally, the inward directed Coriolis momentum pinch is predicted to increase, not decrease, during the ECRH phases. Altogether, the data suggest the presence of either an outward convection of momentum or an intrinsic, counter-current directed torque. Although the physics behind these possibilities remains unclear, they are presumably related to the ECRH-induced changes in the plasma profiles and turbulence. Specifically, the results suggest that the electron and ion temperature profiles are

important parameters in the observed rotation change, possibly through their influence on the plasma turbulence. If this is the case then this effect will probably not contribute to the rotation profiles in large future devices as significant deviations between T_e and T_i will not be possible in these machines. However, as this effect can alter the rotation profiles on current tokamaks it should be kept in mind when using data from present day experiments to extrapolate to future devices.

Acknowledgments

The authors would like to acknowledge the efforts and contributions of the entire ASDEX Upgrade Team. A special thanks goes to the neutral beam and ECRH groups as well as the ECE diagnostic team without whom this work would not have been possible.

[1] J. E. Rice *et al*. Plasma Phys.Control. Fusion, 50:124042, 2008.
[2] A. Bortolon *et al*. Phys. Rev. Lett., 97:235003, 2006.
[3] J. E. Rice *et al*. Nucl. Fusion, 39:1175, 1999.
[4] J. E. Rice *et al*. Nucl. Fusion, 47:1618, 2007.
[5] K. H. Burrell *et al*. Nucl. Fusion, 49:085024, 2009.
[6] H. Biglari, P. H. Diamond, P. W. Terry. Phys. Fluids B, 2:1, 1990.
[7] T. S. Hahm. Phys. Plasmas, 1:2940, 1994.
[8] T. S. Hahm and K. H. Burrell. Phys. of Plasmas, 2:1648, 1995.
[9] K. H. Burrell. Phys. Plasmas, 4:1499, 1997.
[10] P. W. Terry. Rev. Mod. Phys., 72:109, 2000.
[11] E. J. Strait *et al*. Phys. Rev. Lett, 74:2483, 1995.
[12] A. M. Garofalo *et al*. Phys. Rev. Lett., 89:235001, 2002.
[13] H. Reimerdes *et al*. Phys. Rev. Lett., 98:055001, 2007.
[14] H. Reimerdes *et al*. Phys. Rev. Lett., 98:055002, 2007.
[15] R. J. Buttery *et al*. 22nd IAEA Fusion Energy Conference, Geneva Switzerland, 2008.
[16] P. A. Politzer *et al*. Nucl. Fusion, 48:075001, 2008.
[17] N. Oyama *et al*. Plasma Phys. Control. Fusion, 49:249, 2007.
[18] K. D. Zastrow *et al*. Nucl. Fusion, 38:257, 1998.
[19] G. Tardini *et al*. Nucl. Fusion, 49:085010, 2009.
[20] W. Solomon *et al*. Phys. Plasmas, 17:056108, 2010.
[21] M. Yoshida *et al*. Nuclear Fusion, 47:856, 2007.
[22] T. Tala *et al*. Phys. Rev. Lett, 102:075001, 2009.
[23] J. S. deGrassie *et al*. Phys. Plasmas, 11:4323, 2004.
[24] A. Manini *et al*. Nucl. Fusion, 46:1047, 2006.
[25] Y. Lin *et al*. Phys. Rev. Lett., 101:235002, 2008.
[26] M. Yoshida *et al*. Phys. Rev. Lett., 103:065003, 2009.
[27] A. Ince-Cushman *et al*. Phys. Rev. Lett., 102:035002, 2009.
[28] J. E. Rice *et al*. Nucl. Fusion, 49:025004, 2009.
[29] Y. Lin *et al*. Phys. Plasmas, 16:056102, 2009.
[30] J. S. deGrassie *et al*. EPS Conf. on Contr. Fusion and Plasma Phys., ECA 23J:1189, 1999.
[31] S. Ide *et al*. Nucl. Fusion, 47:1499, 2007.
[32] A. Herrmann *et al*. Fusion Sci. Technol., 44:569, 2003.
[33] H. P. Summers. The ADAS User Manual version 2.6, http://adas.phys.strath.ac.uk, 2004.
[34] N. K. Hicks *et al*. Proc. 15^{th} Joint Workshop ECE and ECRH Yosemite, CA, USA, 2008.
[35] R. Fischer. Plasma Phys. Control. Fusion, 45:1095, 2003.
[36] F. Leuterer *et al*. Fusion Sci. Technol., 55:31, 2009.
[37] R. M. Gilgenbach *et al*. Phys. Rev. Lett., 44:647, 1980.
[38] H. Weisen*et al*. Nucl. Fusion, 42:136, 2002.
[39] J. Stober *et al*. Nucl. Fusion, 43:1265, 2003.
[40] C. Angioni *et al*. Nucl. Fusion, 44:827, 2004.
[41] C. Angioni *et al*. Submitted to Nucl. Fusion, 2010.
[42] C. Angioni *et al*. Phys. Plasmas, 12:040701, 2005.
[43] Y. Camenen *et al*. Phys. Plasmas, 16:012503, 2009.
[44] W. A. Houlberg K. C. Shaing S. P. Hirshman *et al*. Phys. Fluids, 17:961, 1997.
[45] R. D. Hazeltine. Phys. Fluids, 17:961, 1974.
[46] S. D. Scott *et al*. Phys. Rev. Lett., 64:531, 1990.
[47] A. Kallenbach *et al*. Plasma Phys. Control. Fusion, 33:595, 1991.
[48] J. S. deGrassie *et al*. Nucl. Fusion, 43:142, 2003.
[49] A. G. Peeters, C. Angioni and D. Strintzi. Phys. Rev. Lett., 98:265003, 2007.
[50] W. Dorland *et al*. Phys. Rev. Lett, 85:5579, 2000.
[51] N. Kluy *et al*. Phys. Plasmas, 12:122302, 2009.

[52] A. G. Peeters and C. Angioni. Phys. Plasmas, 12:072515, 2005.
[53] A. Manini *et al*. Plasma Phys. Control. Fusion, 46:1723, 2004.